RSC Advances

PAPER

View Article Online
View Journal | View Issue

Cite this: *RSC Adv.*, 2021, **11**, 5182

Red wine-inspired tannic acid–KH561 copolymer: its adhesive properties and its application in wound healing†

Chen Chen,[a] Xiao Yang,[b] Shu-jing Li,[a] Feng-jun Ma,[a] Xiao Yan,[a] Yu-ning Ma,*[a] Yu-xia Ma,*[a] Qing-hai Ma,*[b] Shu-zhong Gao[a] and Xiao-jun Huang[c]

Damaged tissue with an open wound is one of the daily injuries and can have different levels of severity. Inspired by the textile dyeing, coloration and skin care effect of pyrogallol-rich red wine, tannic acid–KH561 (TA561) copolymer was fabricated by phenol–silanol reaction and polycondensation of silane in an aqueous medium under mild conditions. This copolymer could undergo sol–gel transition *via* continuous heating or when simply placed at room temperature, during which liquid TA561 oligomers connected with each other to form solid TA561 as a bulk resin or thin film. Combining the advantages of the polyphenols and polysiloxane, TA561 can be used as an adhesive for multiple surfaces, including wood, polytetrafluoroethylene, poly(vinyl chloride), aluminum chips and silicon rubber. Furthermore, TA561 also possessed reducing activity towards Ag^{+} or Au^{3+} ions to form the corresponding nanoparticles. An *in vivo* antimicrobial ability test indicated that TA561 could promote wound healing and showed resistance to methicillin-resistant *Staphylococcus aureus* (MRSA) infection in comparison with KH561. Indeed, TA561 has the potential to be utilized as a low-cost, green bioadhesive material for skin preparations.

Received 27th August 2020
Accepted 2nd January 2021

DOI: 10.1039/d0ra07342c

rsc.li/rsc-advances

1. Introduction

Either triggered by external factors in daily life or underlying diseases, open wounds can give rise to impaired tissue function related syndromes, posing a major threat to human health.[1–3] Open wounds, such as burns and trauma, always create opportunities for various bacterial infections, which may give rise to healing delays and chronic skin defects. Methicillin-resistant *Staphylococcus aureus* (MRSA) is a representative case of a common drug-resistant pathogen recruited to severe wound infections.[4] Efforts have been made to develop novel wound dressings that are able to prevent bacterial infection and simultaneously accelerate the healing speed. Typically, with the aim to keep damaged tissue from drying and provide a temporary closed environment for healing, wound dressings are used to cover the defective tissue while resisting bacterial assault.[5,6] Considering the difference in antibacterial mechanism, universally studied wound dressings include antibiotic-loaded vehicles,[7] nanosilver complexes[8] and antibacterial polypeptides (AMPPs).[9] However, all of the above wound closure methods face limitations in practical use. For instance, bacterial drug resistance might occur during the consecutive and usually redundant release of conventional antibiotics.[10] The wide utilization of nanosilver or silver ions seems to be an effective solution for wound healing. Nonetheless, nanosilver-loaded wound dressings are normally limited by their potential cytotoxicity and hidden dangers of environmental damage.[11] Lastly, although AMPPs have recently been recognized as a promising candidate for a wound dressing material, the wide utilization of AMPPs as antibacterial agents is restricted by their high production cost, liable proteolytic degradation and possibility of sensitization.[12] Against all odds, researchers have turned to bio-mimicking adhesives and summarized the basic characteristics of an ideal medical wound dressing, which include strong adhesion, desirable biocompatibility, low cost, and facile preparation.[13]

It is well-known that long-term intake of polyphenols in red wine could slow down the aging process, lower cholesterol levels and reduce the risk of cardiovascular disease.[14] The mysterious advantages of polyphenols are not only evident in human health, but also in adhesive interfaces, coatings and self-assembled colloids.[15] For example, polyphenols in red wine can deposit on textiles or the surface of containers in which polyphenol-containing liquids are stored. Similarly, these phenomena can also be observed in textile printing and

[a]*Key Laboratory of New Material Research Institute, Department of Acupuncture-Moxibustion and Tuina, Shandong University of Traditional Chinese Medicine, Jinan 250355, China. E-mail: myning0405@163.com; myxia1976@163.com*
[b]*The First Affiliated Hospital of Shandong First Medical University (Shandong Provincial Qianfoshan Hospital), Jinan 250014, China. E-mail: 807317857@qq.com*
[c]*MOE Key Laboratory of Macromolecular Synthesis and Functionalization, Department of Polymer Science and Engineering, Zhejiang University, Hangzhou 310027, China*

† Electronic supplementary information (ESI) available. See DOI: 10.1039/d0ra07342c

Table 1 The ingredients and reaction process leading to the TA561 copolymer

Sample name	Tannic acid (g)	KH561 (mL)	Trizma base (g)	Water (mL)	Molar ratio (tannic acid/KH561)	Reaction time[a] (min)	Gel time (min)
KH561 under alkaline condition	0	10	0.2	4	0	—[b]	—[b]
TA561-1	1	10	0.2	4	0.016	—[b]	—[b]
TA561-2	2	10	0.2	4	0.032	100	480
TA561-3	3	10	0.2	4	0.048	80	540

[a] Denotes the time taken to obtain the homogeneous liquid copolymer. [b] Denotes that a precipitate was produced during preparation.

coloration processes, which can be ascribed to multiple physical or chemical interactions between the polyphenol and various interfaces. As one of the most common polyphenols in daily life, tannic acid (TA), bearing five digallic acid units ester-linked to a glucose core, has the ability to form complexes or networks through multiple site binding.[16] Moreover, TA is an important commercial raw material, normally used as the tanning agent in the leather industry, as well as in coating, adhesive, cosmetic, pharmaceutical and food addictive applications.[17] Compared with mussel-inspired polydopamine, an abundant source of TA can be found in numerous kinds of plants and TA has also garnered significant research interest as a low-cost dopamine analogue.[18] Furthermore, TA coating takes less time on almost all organic and inorganic surfaces in comparison with the process of dopamine coating.[19] Thus, tannic acid is an ideal crosslinker leading to the production of organic–inorganic hybrid materials with synergistic properties to meet complex biological requirements, such as those for wound dressings.[20–22]

Recently, the dehydration reactions between the hydroxyl groups of polyphenol and the Si–OH groups of silane have been studied by various researchers. The corresponding organic–inorganic hybrid materials are promising in fields including silicon rubber, anti-corrosion coatings for metal surfaces and modified graphene electrodes.[23–25] He *et al.* chose γ-(2,3-epoxypropoxy)propyltrimethoxysilane (KH560) to modify graphene–TA complexes through a polyphenol–silanol reaction,[25] and the resulting composite coatings exhibited enhanced anti-corrosion properties over those of Gr–TA/epoxy, as well as pure epoxy. However, the hydrolysis of KH560 could generate methanol, so it is not suitable for biomedical uses. Herein, we pioneered the simple construction of a red wine inspired copolymer, in which tannic acid and low-toxicity KH561 were crosslinked together by the dehydration reactions between TA and γ-(2,3-epoxypropoxy) propyltriethoxysilane (KH561), as well as silane hydroxyl condensation. The chemical structure of the resulting copolymer, TA hardened KH561 (TA561), was confirmed by Fourier transform infrared spectroscopy (FT-IR). Further characterization showed that TA561 had the ability to reduce noble metal ions, scavenge free radicals and adhere well to multiple surfaces owing to the incorporation of polyphenol groups. Moreover, the *in vivo* antimicrobial ability of TA561 was studied with a MRSA-infected wound model, in which pathogen-free BALB/c immune-competent male mice were used. Finally, by merging the merits of polyphenol and polysiloxane, this organic–inorganic hybrid material is promising in adhesives, catalysts, photo-thermal conversion and wound healing.

2. Experimental section

2.1. Materials

Tannic acid (TA) and $HAuCl_4$ were purchased from Aladdin Co., Shanghai, China. KH561 was received from Bolian Chemical Co., Zhengzhou, China. Trizma base (primary standard and buffer, ≥99.9% titration, crystalline) and DMSO were purchased from Sigma-Aldrich. $AgNO_3$ was purchased from Ourchem Co., Shanghai, China. 1,1-Diphenyl-2-picrylhydrazyl (DPPH) was purchased from Macklin Co., Shanghai, China. Minimum Essential Medium (MEM) was obtained from Hyclone (USA). 3-(4,5-Dimethylthiazol-2-yl)-2,5-diphenyltetrazolium bromide (MTT) and calcein/propidium iodide (PI) cell viability/cytotoxicity assay kits were purchased from Beyotime Biotechnology (Shanghai China). PBS solution was obtained from Sunshine Bio (Nanjing, China). Heat-inactivated horse serum was purchased from Gibco (USA). GlutaMAX, sodium pyruvate and non-essential amino acids were purchased from Invitrogen Corporation (USA). All other reagents were commercial chemicals and used as received, unless otherwise indicated.

2.2. Preparation of TA561 copolymer

The detailed preparation procedures of the TA561 copolymer can be described as follows. Firstly, in a 50 mL plastic centrifugal tube, a certain amount of tannic acid and 200 mg Trizma base were fully dissolved in 4 mL distilled water. Then, 10 mL KH561 was added to the above mixture under vigorous stirring at 60 °C. After 80–100 min of stirring, the liquid TA561 copolymer was obtained as a homogeneous brown viscous solution. Finally, this copolymer, could be directly used without any purification process, and was stored at 4 °C. Meanwhile, TA561-*n* denotes that *n* grams of TA was used to synthesize TA561 (Table 1).

2.3. Sol–gel transition of the TA561 copolymer

For the preparation of solid TA561, the liquid TA561 copolymer was poured into polypropylene molds, put into an oven and heated for another 7–8 h to obtain solid TA561 disks. After that, the disks were washed with ethanol and water several times before use.

2.4. *In situ* formation of Au and Ag NPs on TA561

The volume of each solid TA561 disk was 2 mL, with a bottom diameter of 2.5 cm. For the formation of Au NPs, the TA561 solid disks were directly immersed into $HAuCl_4$ aqueous solution (0.05 wt%, 10 mL) under constant shaking for 10 min. Similarly, a $AgNO_3$ aqueous solution (0.1 wt%, 10 mL) was utilized to form Ag NPs. The whole process was recorded by a UV-Vis spectrophotometer (UV2450, Shimadzu, Japan).

2.5. Methods for adhesive tests

The liquid TA561 copolymer was deposited onto substrates such as wood, aluminum (Al) chips, poly(vinyl chloride) (PVC), silicon rubber (SR) and even polytetrafluoroethylene (PTFE). The deposition area was set as 2.5 cm × 2.5 cm. Then another substrate was used to press the deposited copolymer liquid at room temperature for 24 h. The shear strength experiments were tested on a HY-0580 tension machine (HENGYI Company). The two substrates were adhered between the two fixtures in the vertical direction. The strain rate was 100 mm min^{-1}, and the data were collected until the separation of the two substrates. The adhesive properties after water immersion treatment were investigated as follows. Typically, the already agglutinated substrates were immersed in a water bath at 60 °C for 1 h, and then shear strength experiments were also performed to similarly test the adhesive properties.

2.6. Antioxidant activity of TA561

The DPPH radical (DPPH$^{\cdot}$) scavenging method was used to assess the antioxidant ability of TA561, in reference to a previously studied method.[26] The addition of DPPH$^{\cdot}$ would trigger a polyphenol-based reduction reaction, causing a color change from violet to pale yellow. The efficiency of the antioxidant activity was determined as follows: dried solid TA561 disks with a volume of 2 mL were immersed in a 50 mL centrifugal tube containing 30 mL of 0.15 mM DPPH/methanol solution. The absorbance at 517 nm was recorded using a UV-Vis spectrophotometer after the solutions had been allowed to stand in the dark for 30 min. A sharp decline in absorbance value at 517 nm exhibited high DPPH radical scavenging activity. The DPPH-scavenging activity could be obtained using the formula below:

$$\text{DPPH-scavenging activity } (\%) = \left(\frac{A_c - A_s}{A_c}\right) \times 100\%$$

In this equation, A_s and A_c are the absorbance of the sample and of the blank control at 517 nm, respectively.

2.7. *In vivo* wound healing properties of TA561

All animal studies were carried out according to the National Institutes of Health Laboratory Animal Care and Use Guidelines (NIH publication no. 85-23 rev. 1985) and experiments were approved by the Animal Ethics Committee of Shandong University of Traditional Chinese Medicine. This article does not contain any studies with human participants performed by any of the authors.

C57BL/6 mice are commonly used in oncology, physiology, immunology and genetics.[27–29] Herein, six to eight week old C57BL/6 male mice (18–22 g) were used as an *in vivo* MRSA infection model. The mice were separated into three groups, including blank control, KH561 and TA561-3 with each group containing 3 mice ($n = 3$). Before the test, all mice were exposed to a 12 h light–12 h dark period in a chamber. The temperature was set as a constant 21 ± 1 °C with a relative humidity of 60 ± 5% for at least 7 days. Then, the mice were anaesthetized by intraperitoneal injection of a ketamine (10%) and xylazine (5%) mixture. Then the dorsal area of the rats was shaved by a razor and cleaned with alcohol. A disposable biopsy punch was used to create a full-thickness round open wound (diameter = 6 mm) on the back. The wounds were injected with *S. aureus* (3×10^7 CFU, 50 μL) and different treatments were used for the wounds of the mice at each 24 h interval. The volume of KH561 or TA561-3 used for wound daubing was 200 μL. Photographs of the resulting wounds, together with the diameters of the wounds, were recorded each day. The wounds of the mice were excised at the seventh day and placed in sterile saline (1 mL). Then, bacterial samples were collected from the wounds after incubation for 24 h at 37 °C.

2.8. Skin sensitivity test

Six 7 week-old BALB/c male mice were exposed to a 12 h light–12 h dark period in a chamber. The temperature was set as a constant 21 ± 1 °C with a relative humidity of 60 ± 5% for at least 7 days. Then, a 10% chloral hydrate solution was used for abdominal anesthesia at a dose of 3 mL kg^{-1} and the backs of the mice were shaved with a razor. Liquid TA561 copolymer (200 μL) was daubed onto the back skin. The daubed area was cover with two layers of gauze and a layer of glass beads, then sealed and fixed with non-irritating adhesive tape for 3 days.

2.9. *In vivo* biosafety of TA561

Typically, TA561 (12 mg kg^{-1}) was administrated into BALB/c male mice *via* intraperitoneal injection ($n = 4$). Blood samples were collected from the mice at the seventh day of treatment for blood biochemistry examination. Major organs, including the heart, liver, spleen, lungs and kidneys, were collected from the mice after seven days of treatment for pathological examination. In addition, the control mice (treated with PBS buffer) and the tannic acid-treated mice were also sacrificed after 7 days of therapy. The major organs were harvested from both groups and were also pathologically examined.

2.10. Cytotoxicity *in vitro*

2.10.1. Cell culture. L929 fibroblast cells were obtained from ATCC. These cells were cultured in MEM supplemented with 10% heat-inactivated horse serum, GlutaMAX (1%), sodium pyruvate (100 mM, 1%) and non-essential amino acids (diluted 100 fold, 1%) in an incubator (5% CO_2, 37 °C). Once they reached the logarithmic phase, the cells were collected using centrifugation at 1000*g* for 5 min.

2.10.2. *In vitro* cytotoxicity. Cells were suspended in MEM and seeded into a 96-well plate (3×10^3 cells per well), and incubated for 24 h (37 °C, 5% CO_2) to harvest a monolayer of

cells. After removing the MEM, extracts (obtained from tannic acid, KH561 and TA561 with MEM) with various concentrations (6.25 μg mL^{-1}, 12.5 μg mL^{-1}, 25 μg mL^{-1}, 50 μg mL^{-1}, 100 μg mL^{-1} and 200 μg mL^{-1}) were added to the above wells. After 24 h, 10 μL of MTT (5 mg mL^{-1}, in PBS) was added to the corresponding wells, allowing formazan crystals to form for another 3 h. Subsequently, the culture medium was carefully removed, and replaced with 150 μL DMSO to dissolve the formazan for 10 min. The absorbance of each well was measured at 570 nm (reference 650 nm). Cells treated with MEM were taken as the negative control. Relative cell viability was obtained using the following equation:

$$\text{Relative cell viability } (\%) = \frac{OD_{test}}{OD_{control}} \times 100\%$$

2.10.3. Fluorescence staining of living cells. L929 cells treated with different extracts from tannic acid, KH561 and TA561 were qualitatively distinguished by fluorescence staining using calcein or PI. Typically, L929 cells were seeded in culture wares (3.5 cm in diameter, 1×10^6 cells per ware). Extracts of tannic acid, KH561 and TA561 (40 μg mL^{-1}) were added to the cells and incubated for 24 h. Thereafter, the media were removed. L929 cells were incubated with 250 μL diluted calcein/PI solution (10^3 fold) for 5 min after washing with PBS three times. Cells without any treatment were used as the negative control. Finally, the cells were observed by a fluorescence microscope (Zeiss, LSM710).

3. Results and discussion

Inspired by the desirable coating properties of pyrogallol-rich solutions such as red wine, coffee, and tea, TA was chosen to generate a brand-new copolymer for adhesive as well as wound dressing applications. As illustrated by Scheme 1 and Table 1, TA and KH561 were used to synthesize a tannic acid–epoxy silane (TA561) copolymer, in which tannic acid acted as the crosslinker, KH561 acted as the monomer and Trizma base acted as the catalyst. Since TA561 contains both pyrogallol residues and alcohol originating from the hydrolysis of KH561, the color as well as the smell of this mixture were similar to red wine. The whole synthetic procedure avoided using toxic organic solvents and harmful substances, which was in conformity with the requirements of green chemistry.

As can be seen in Fig. 1, FI-IR spectroscopy was carried out to investigate the chemical composition of the TA561 copolymer. After the polymerization process, a new adsorption peak appeared at 1038 cm^{-1}, assigned to Si–O–Si asymmetric vibration. In the meantime, the adsorption peak of Si–OR stretching at 955 cm^{-1} vanished after polymerization. Two new absorption peaks appeared at 2940 cm^{-1} and 2875 cm^{-1} that were assignable to the $-CH_3$ and $-CH_2$ groups of KH561, implying successful crosslinking between tannic acid and KH561 accompanied by hydrolytic condensation of silane. Moreover, the tannic acid segment showed a broad absorption band near 3400 cm^{-1} that is assigned to phenolic –OH. Meanwhile, some strong bands typical of polyphenols assigned to C=O stretching at 1716 cm^{-1}, benzyl stretching at 1613, 1534 and 1448 cm^{-1}, C–O stretching at 1200 cm^{-1}, and trisubstituted benzene ring scissoring at 759 cm^{-1} (the yellow region in Fig. 1) were observed. Inherent from KH561, the adsorption peaks at 908 cm^{-1} and 1080 cm^{-1} were assignable to epoxy residues and Si–O–C (the blue region in Fig. 2), which revealed that TA561 is an organic–inorganic hybrid polymer containing the main functional groups derived from tannic acid and KH561.

The synthesized TA561, at first, was a red wine-like liquid copolymer. Interestingly, this copolymer could undergo a sol–gel transition after a continuous heating process. The changes in viscosity as well as variation of the chemical structure during the sol–gel transition can be seen in Fig. 2. KH561 cannot form a viscous solution and exhibited no sign of sol–gel transition during the whole observation period (the dotted line in Fig. 2a). This phenomenon could be attributed to linear polysiloxane through silane hydrolysis and hydroxyl condensation of KH561

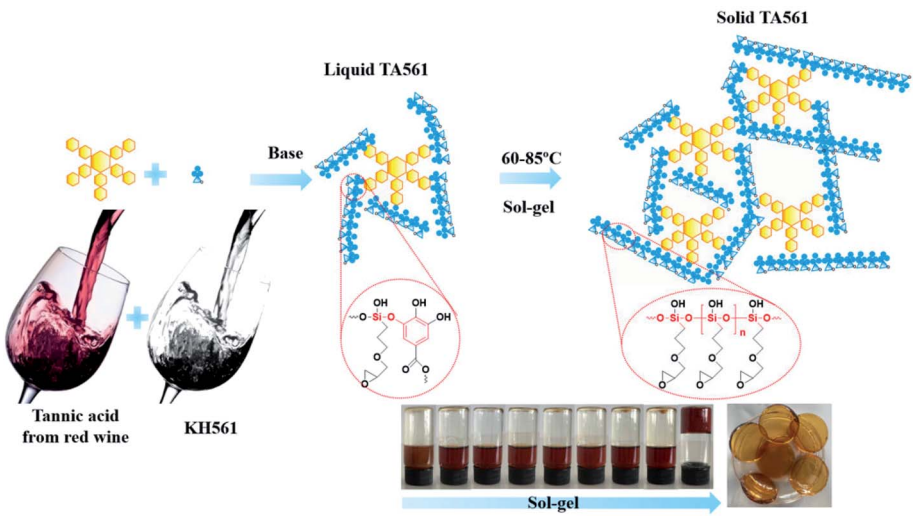

Scheme 1 Synthetic process of the TA561 copolymer.

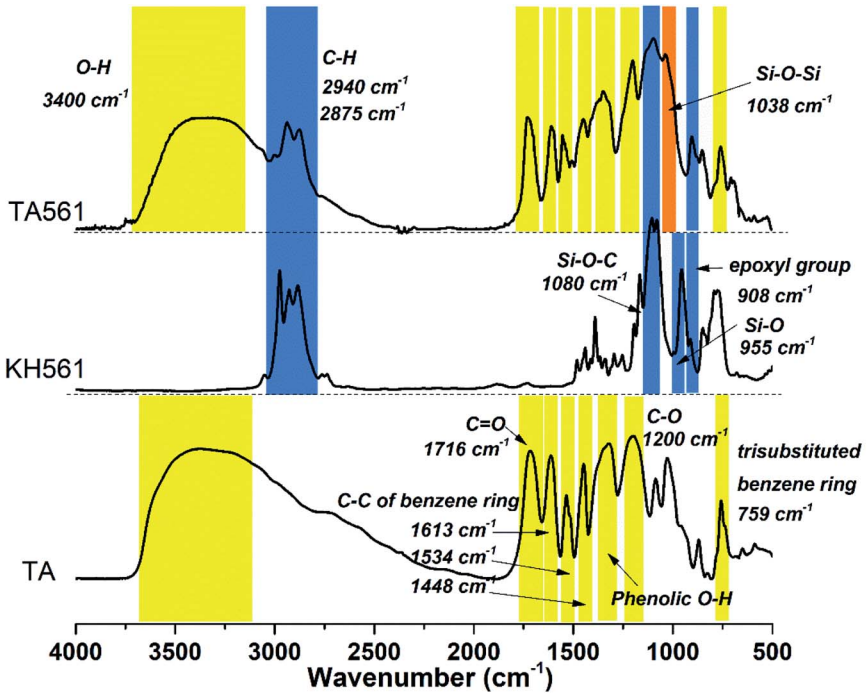

Fig. 1 FT-IR spectra of TA, KH561 and TA561 copolymer.

under basic conditions. In the case of TA561-2 and TA561-3, the viscosity stayed constant at first, followed by a sharp increase during the sol–gel transition. In the presence of TA as a cross-linker, a polymeric network finally formed between TA and the linear polysiloxane derived from KH561. In order to analyze the competition of the two related reactions, the polyphenol–silanol dehydration reaction together with the silane poly-condensation, the chemical structures of the TA561 copolymer at different heating times were viewed by FT-IR spectroscopy, as shown in Fig. 2b. It is obvious that the initial adsorption peak of

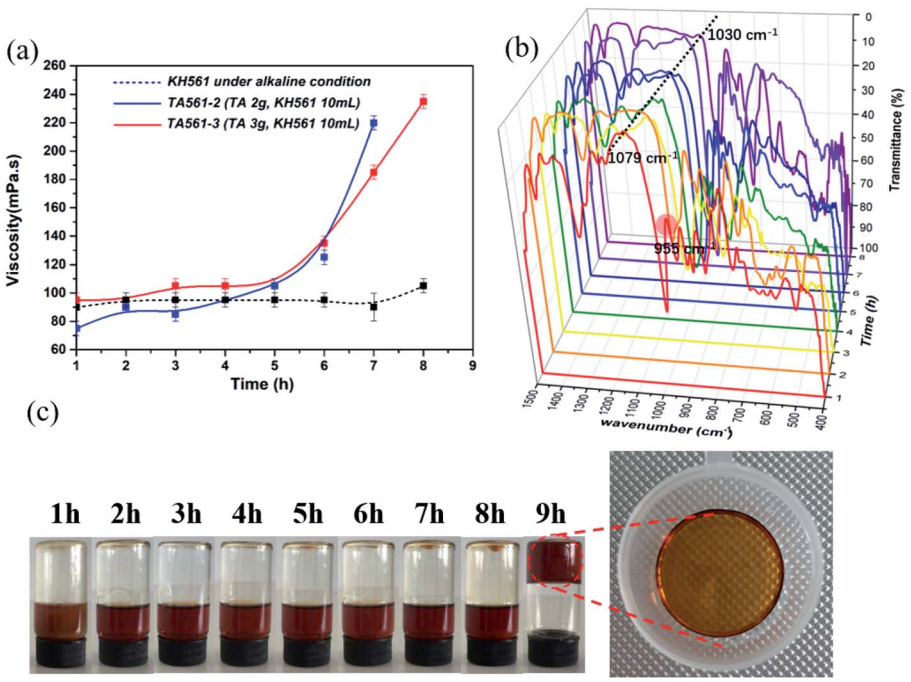

Fig. 2 The viscosity and change in chemical structure during sol–gel transition of TA561 copolymer. (a) The viscosity of KH561, TA561-2 and TA561-3 as a function of time. (b) The chemical structures of TA561-3 under different heating times at 60 °C (1 h, 2 h, 3 h, 4 h, 5 h, 6 h, 7 h, 8 h and 9 h) viewed by FT-IR spectroscopy. (c) Pictures of the morphology of TA561-3 during sol–gel transition.

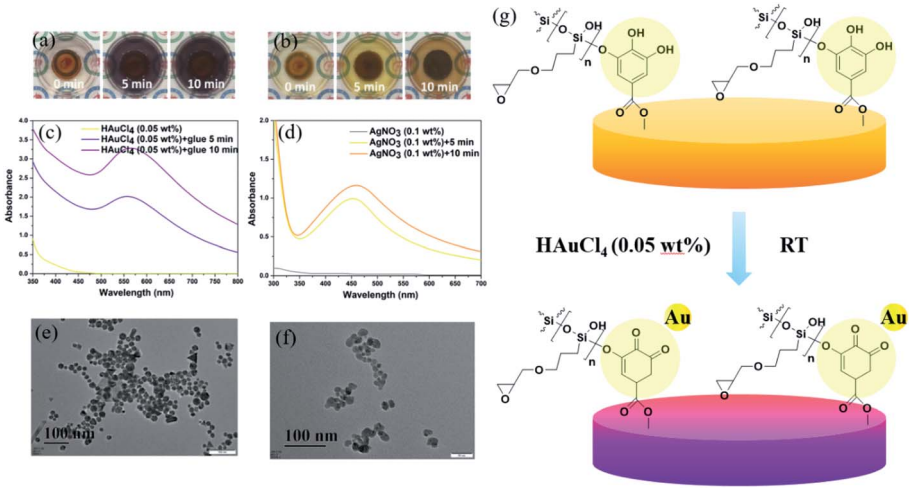

Fig. 3 The formation of Au & Ag NPs by using a solid TA561 disk as a reductant. (a) Photographs of a solid TA561 disk during treatment with $HAuCl_4$ (0.05 wt%). (b) Photographs of a solid TA561 disk during treatment with $AgNO_3$ (0.1 wt%). (c) Formation of Au NPs as indicated by the UV-Vis spectrum. (d) Formation of Ag NPs as indicated by the UV-Vis spectrum. (e) The morphology of the Au NPs viewed by TEM. (f) The morphology of the Ag NPs viewed by TEM. (g) Schematic process for the formation of the Au NP-decorated TA561 copolymer.

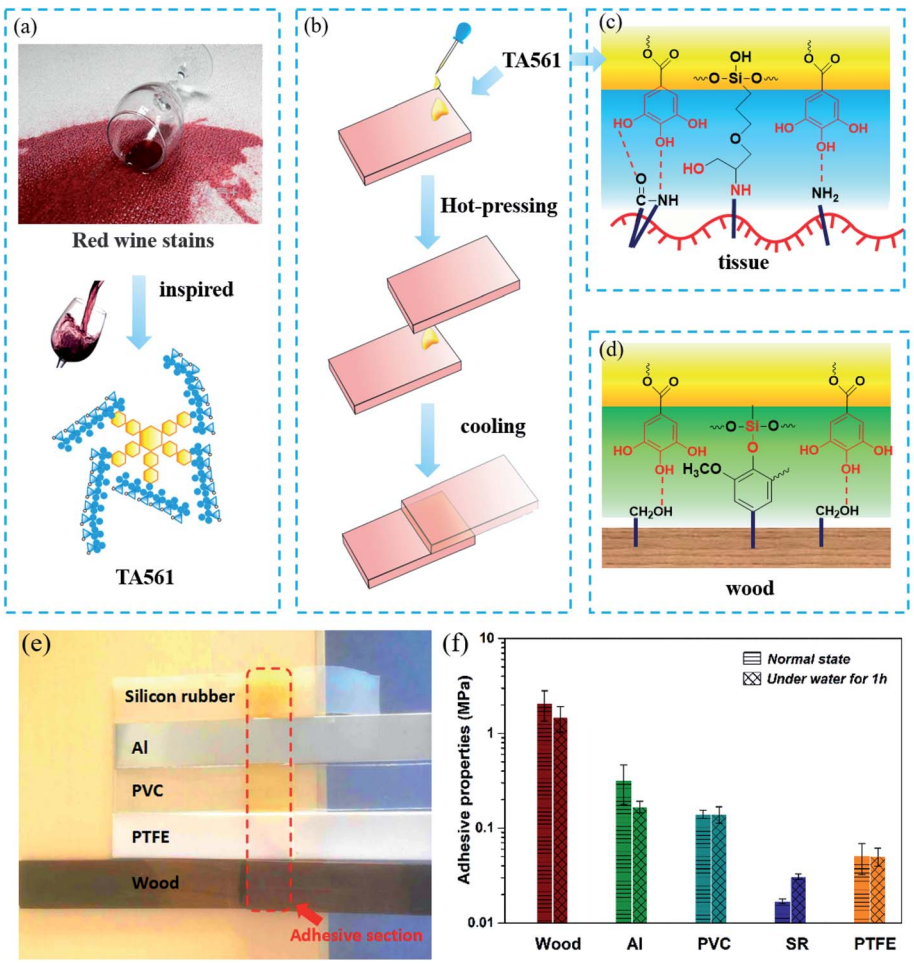

Fig. 4 Application of the red wine-inspired TA561 copolymer as an adhesive material. (a) TA561 copolymer mimics a red wine stain. (b) Schematic representation of the adhesion procedure. (c) The adhesive behavior for the TA561–tissue interface. (d) The adhesive behavior for the TA561–wood interface. (e) Photograph of various materials agglutinated by TA561 copolymer; the adhesive section area was fixed as 2.5 cm × 2.5 cm. (f) Shear strengths on five different types of surfaces, including wood, aluminum, poly(vinyl chloride), silicon rubber and polytetrafluoroethylene (error bars present the SDs with $n = 6$ repeats).

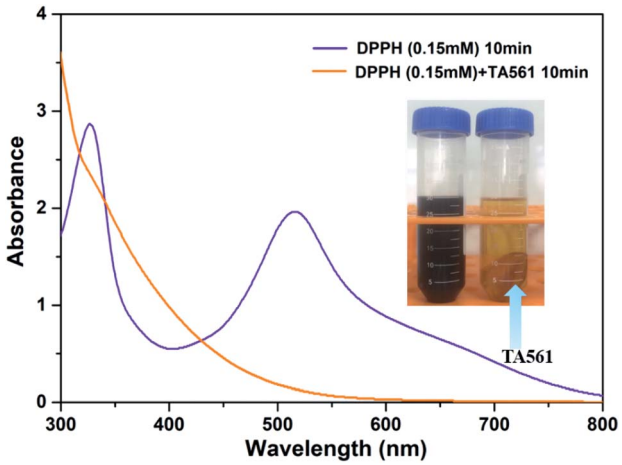

Fig. 5 Antioxidant ability of a solid TA561 disk (TA561 gel) after 10 min of incubation of DPPH solution (0.15 mM in methanol).

Si–OR stretching at 955 cm^{-1} vanished after 2 h, which indicated the successful dehydration reaction between tannic acid and KH561. Furthermore, the absorption peak assigned to Si–O–Si at 1079 cm^{-1} remained still at 0–5 h. However, this absorption peak red shifted to 1030 cm^{-1} on prolonging the heating time, which resulted from the elongation of the polysiloxane backbone after successive silane hydroxyl condensation. It should be noted that the viscosity increase coincided with chain growth of polysiloxane. As can be seen in Fig. 2c, the solution of the TA561 copolymer finally gelled after 9 h of heating at 60 °C. Above all, it could be inferred from the results that KH561 was first hydrolyzed and reacted with TA *via* dehydration reactions between the hydroxyl groups of the pyrogallol residues and the silanol groups, which gave rise to liquid TA561 oligomers. When the liquid TA561 was subjected to constant heating, chain growth of polysiloxane occurred and finally a polymeric network formed to give solid TA561. In the absence of heating, the time taken for sol–gel transition was up to one week at room temperature. Such sol–gel transition behavior of TA561 could enable the construction of functional coatings for multiple uses, considering the unique properties of TA and KH561.

TA is a natural reducing agent extracted from plant sources, which is capable of chelating with some metal ions and reducing them to metallic nanoparticles (NPs).[30,31] After the crosslinking process, the TA561 copolymer inherited catechol units from TA, ready for metal ion reduction reactions. As illustrated by Fig. 3a, it is obvious that the gel color changed to dark crimson within 5 min due to the formation of Au NPs. Similarly, when Ag^{+} ions diffused into TA561, the gel color changed to dark brown within 5 min under room temperature indicating the formation of Ag NPs in Fig. 3b. Moreover, the ultraviolet and visible (UV-Vis) spectrum was also obtained to analyze the corresponding metal reduction process. As seen in Fig. 3c, a strong absorption peak concerning Au NPs at

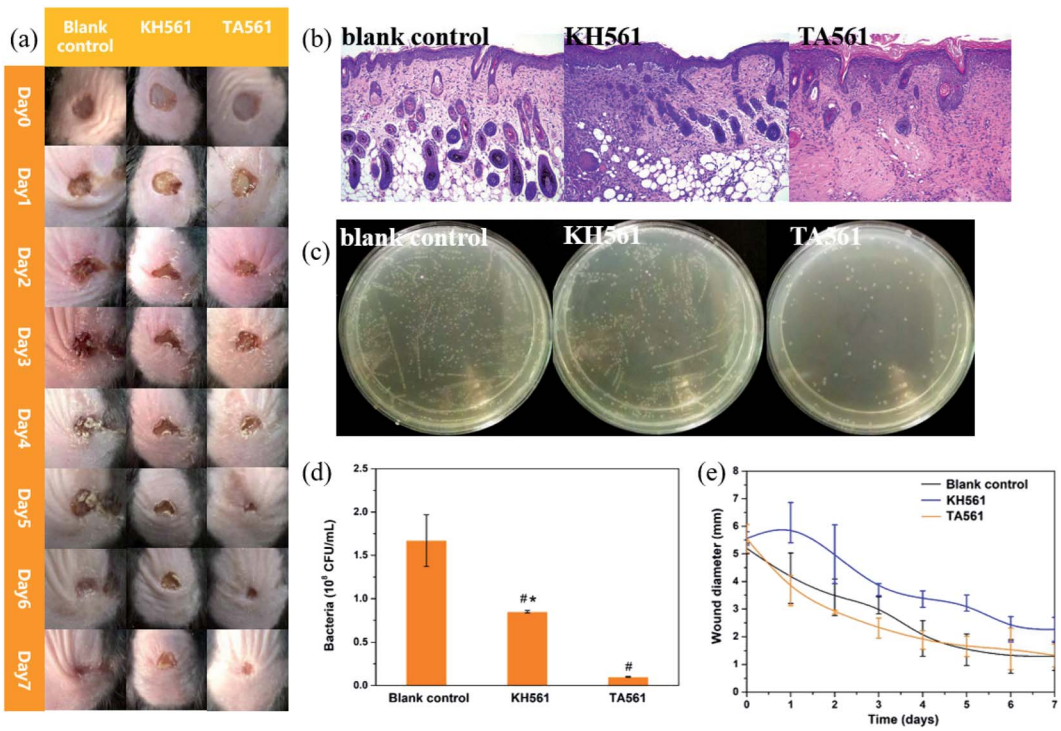

Fig. 6 *In vivo* antimicrobial ability test. (a) Photographs of *S. aureus* infected wounds of mice at different times. (b) Corresponding H&E-stained histologic section of a wound. (c) Photographs of bacterial colonies obtained from wound tissue. (d) The surviving bacteria in the wound were quantified. The error is the standard deviation from the mean ($n = 3$). *Significantly different ($P < 0.05$) and #significantly different ($P < 0.1$) from data obtained. (e) Wound sizes as a function of time.

approximately 540 nm showed up, which could be ascribed to the surface plasmon resonance (SPR) effect of Au NPs. As to the formation of Ag NPs, an indistinct band appeared at 452 nm within 5 min, probably corresponding to the SPR effect of spherical silver nanoparticles (Fig. 3d). In addition to the tailing effect, this peak broadened and slightly shifted to 461 nm with lengthened reduction time, revealing that larger Ag NPs came into being. The morphologies of the Au and Ag NPs were viewed using TEM photographs. Interestingly, the Au NPs were triangular, hexagonal, cylindrical, spherical and even rhombic in shape, as shown in Fig. 3e, suggesting that the resulting nanoparticles were generally nanocrystals. Considering that there was no heating operation, inorganic salt or surfactant in this reduction process, the diversity in shape could be ascribed to variation in the Au^{3+} concentration around the TA561 gel during the rapid formation of Au NPs.[32] It can be clearly seen from Fig. 3f that the Ag NPs are generally spherical in shape with a mutable size ranging from 8 to 20 nm. Overall, Fig. 3g presents a schematic diagram to illustrate the *in situ* formation of the Au NP-decorated TA561 gel, in which the polyphenol groups were oxidized to quinone groups while the metal precursors were reduced to nanoparticles.[33] The whole reduction reaction proceeded in an aqueous solution under ambient conditions, and so it is a facile method for the rapid generation of noble metal NPs (see Movies S1 and S2†).

In normal life, the stains on textiles caused by red wine are usually hard to wash away as the TA-based phenolic coating offers sufficient sites to anchor on flexible surfaces (Fig. 4a). As illustrated by Fig. 4b, the TA561 liquid copolymer was deposited on one piece of a given slice, consequently pressed with another piece of the same slice at room temperature and stood for 24 h. Owing to the abundant polyphenol residues in the TA561 copolymer, the tendency to form intermolecular hydrogen bonds with the given surfaces made this copolymer a potential surface adhesive. Moreover, the introduction of TA561 provides quantitative epoxy groups, which could bind the tissue and wood surface by epoxy chemistry and thus give enhanced binding affinities (Fig. 4c and d). As can be seen in Fig. 4e, materials such as wood, aluminum (Al), poly(vinyl chloride) (PVC), silicon rubber (SR) and even polytetrafluoroethylene (PTFE) were agglutinated by liquid TA561. The results in Fig. 4f exhibited that the resultant copolymer exhibited a reliable adhesive capability to wood with a shear strength up to 2.00 MPa, in which both the high-density H-bonds and the newly formed silicon–oxygen bonds between TA561 and lignin strengthened the adhesion. Liquid TA561 copolymer was also able to adhere to hydrophobic PTFE surfaces with a shear strength of 0.05 MPa owing to hydrogen bonding between the polyphenol groups of TA561 and the fluorine atoms of the hydrophobic PTFE surface. The TA561 copolymer also showed affinity to Al surfaces with a shear strength of 0.14 MPa since the polyphenol–metal interactions played a critical role. Additionally, the agglutinated samples were further subjected to heating under water at 60 °C for 1 h. It is interesting that the adhesive shear strength for SR was 0.02 MPa before the water immersion procedure. However, this value increased to 0.03 MPa after immersion in the water bath, probably due to the silane hydroxyl condensation reaction between the silanol groups from both sides. Though glass was also chosen in adhesive tests, the corresponding shear strength was ultrahigh because the breakage occurred by stretching before the TA561 agglutinated glass slices separated. Thus, TA561 has potential to be applied as an adhesive for various materials.

The ability to scavenge DPPH radicals ($DPPH^{\bullet}$) could reveal the antioxidant activity of the TA561 copolymer. For decades, pyrogallol-rich drinks such as red wine have earned persuasive attention due to their beneficial efficacy in antiaging, as antioxidants and in free radical trapping. Meanwhile, persistent intake of red wine lowers the risk of pathologies including cancer and cardiovascular disease.[34,35] As can be seen in Fig. 5, a deep violet DPPH solution centered at 517 nm gradually changed to a colorless pale yellow solution upon the addition of TA561, which resulted from $DPPH^{\bullet}$ neutralization. Overall, the antioxidant ability of the TA–PEG hydrogel was up to 95% after 10 min of incubation of DPPH solution.

Compared with male animals, female animals have completely different hormone profiles. This makes the monthly changes of estrogen and progesterone in female mice very obvious, while testosterone in male mice remains at a high level for a long time. So it is considered that male animals can give more stable data. Moreover, estrogen has certain anti-inflammatory effects, which makes it hard to predict the wound healing properties of the provided wound dressings.[36,37] Thus, only male mice were used in this study. As shown in Fig. S1a,† intact skin could be observed after TA561 daubing for 1 d, 2 d and 3 d. Meanwhile, the H&E-staining result justified the absence of skin inflammation reactions (Fig. S1b†). With an aim to further estimate the wound healing ability, the *in vivo* antimicrobial ability of the TA561 copolymer and KH561 was tested with a MRSA wound infection model. As can be seen in Fig. 6a, full thickness open wounds (area 1.1 cm^2) were created on the back of C57BL/6 male mice. In comparison with the blank control and KH561, the wounds of the mice treated by TA561 copolymer became abnormally smaller during the observation time. To further evaluate the wound healing ability, histological analysis alongside hematoxylin and eosin (H&E) staining was conducted (Fig. 6b). At day 7 after incubation, large amounts of inflammatory cells and imperfect epidermal layers appeared in the blank control as well as the KH561 groups. In contrast, a mostly intact epidermis structure and just a few inflammatory cells were observed in the TA561 groups. The sterilization efficiency was also evaluated as illustrated by Fig. 6c and d, in which the wounds of the mice were excised at the seventh day to determine the related antibacterial ability. As a result, bacteria in the TA561 groups decreased to 1.6%, which indicated that TA561 significantly showed resistance to wound infection. In contrast, KH561 also exhibited a degree of antibacterial activity. However, the amount of bacteria only decreased to 14.5%. In all groups, the size of the wound tended to decease as a function of time after treatment (Fig. 6e). Reduction of the wound area was the accelerated in the TA561 group. The therapeutic effect in the KH561 group remained inapparent compared with the other two groups, possibly due to

its relatively weak antibacterial ability and rigid film-forming properties.

Though TA561 had desirable adhesive and wound healing properties, the *in vivo* toxicity test indicated that this copolymer could induce a negative effect on the kidney and liver function and cause weight loss of the mice during 7 days of treatment (Fig. S2–S8†). The toxicity of TA561 cannot be avoided due to the introduction of an epoxy functional group.[38] The *in vitro* cytotoxicity test showed that TA561 had a negative effect on cell proliferation, especially at high concentrations above 25 μg mL^{-1} (Fig. S9 and S10†). As a kind of polyepoxy material, TA561 copolymer could give rise to the inhibition of tissue cellular activity and even tissue fixation.[39] Therefore, more dedicated work focused on reducing the side effects of TA561 should be initiated to fulfill the practical requirements.

4. Conclusion

In summary, red wine-mimicking TA561 copolymer was fabricated by a polycondensation reaction between tannic acid and KH561, in which a polyphenol–silanol dehydration process was conducted prior to silane polycondensation. Bearing polyphenol groups, TA561 can reduce Ag^{+} and Au^{3+} ions to the corresponding nanoparticles under ambient conditions. Taking advantage of the TA-based phenolic coating on a flexible surface, the TA561 copolymer could be used as an adhesive for daily used materials such as wood, polytetrafluoroethylene, poly(vinyl chloride), aluminum chips and silicon rubber. Moreover, the TA561 copolymer also exhibited free radical scavenging properties as evidenced by DPPH assay. The results from an *in vivo* antimicrobial assay against MRSA indicated that the TA561 copolymer could be a facile treatment for wound healing in contrast to KH561. Therefore, this copolymer is promising in areas such as adhesives, catalysts, photo-thermal conversion materials and wound healing.

Conflicts of interest

The authors declare that they have no conflict of interest.

Acknowledgements

The study was supported by the National Natural Science Foundation of China (grant no. 81373721).

References

1 B. Yu, S. Y. Kang, A. Akthakul, N. Ramadurai, M. Pilkenton, A. Patel, A. Nashat, D. G. Anderson, F. H. Sakamoto, B. A. Gilchrest, R. R. Anderson and R. Langer, *Nat. Mater.*, 2016, **15**, 911–918.
2 M. G. Jeschke, D. L. Chinkes, C. C. Finnerty, G. Kulp, O. E. Suman, W. B. Norbury, L. K. Branski, G. G. Gauglitz, R. P. Mlcak and D. N. Herndon, *Ann. Surg.*, 2008, **248**, 387–400.
3 D. Church, S. Elsayed, O. Reid, B. Winston and R. Lindsay, *Clin. Microbiol. Rev.*, 2006, **19**, 403–406.
4 A. S. Lee, H. de Lencastre, J. Garau, J. Kluytmans, S. Malhotra-Kumar, A. Peschel and S. Harbarth, *Nat. Rev. Dis. Primers*, 2018, **4**, 18033–18063.
5 S. A. Castleberry, B. D. Almquist, W. Li, T. Reis, J. Chow, S. Mayner and P. T. Hammond, *Adv. Mater.*, 2015, **28**, 1809–1817.
6 E. J. Lee, B. K. Huh, S. N. Kim, J. Y. Lee, C. G. Park, A. G. Mikos and Y. B. Choy, *Prog. Mater. Sci.*, 2017, **89**, 392–410.
7 M. Kumar, S. Jaiswal, K. K. Sodhi, P. Shree, D. K. Singh, P. K. Agrawal and P. Shukla, *Environ. Int.*, 2019, **124**, 448–461.
8 N. R. Panyala, E. M. Pena-Mendez and J. Havel, *J. Appl. Biomed.*, 2008, **6**, 117–129.
9 Y. Q. Zheng, Y. Luo, K. Feng, W. D. Zhang and G. J. Chen, *ACS Macro Lett.*, 2019, **8**, 326–330.
10 M. Xu, A. Khan, T. J. Wang, Q. Song, C. M. Han, Q. Q. Wang, L. L. Gao, X. Huang, P. Li and W. Huang, *ACS Appl. Bio Mater.*, 2019, **2**, 3329–3340.
11 S. Marin, G. M. Vlasceanu, R. E. Tiplea, I. R. Bucur, M. Lemnaru, M. M. Marin and A. M. Grumezescu, *Curr. Top. Med. Chem.*, 2015, **15**, 1596–1604.
12 M. Zasloff, *Nature*, 2002, **415**, 389–395.
13 J. Deng, Y. Y. Tang, Q. Zhang, C. Wang, M. Liao, P. Ji, J. L. Song, G. X. Luo, L. Chen, X. H. Ran, Z. M. Wei, L. W. Zheng, R. Y. Dang, X. Liu, H. M. Zhang, Y. S. Zhang, X. M. Zhang and H. Tan, *Adv. Funct. Mater.*, 2019, **29**, 1809110.
14 V. Nash, C. S. Ranadheera, E. N. Georgousopoulou, D. Mellor, D. B. Panagiotakos, A. McKune, J. Kellett and N. Naumovski, *Food Res. Int.*, 2018, **113**, 277–287.
15 F. Reitzer, M. Allais, V. Ball and F. Meyer, *Adv. Colloid Interface Sci.*, 2018, **257**, 31–41.
16 W. Zhang, R. X. Wang, Z. M. Sun, X. W. Zhu, Q. Zhao, T. F. Zhang, A. Cholewinski, F. Yang, B. X. Zhao, R. Pinnaratip, P. K. Forooshanie and B. P. Lee, *Chem. Soc. Rev.*, 2020, **49**, 433–464.
17 S. Z. Moghaddam, S. Sabury and F. Sharif, *RSC Adv.*, 2014, **4**, 8711–8719.
18 C. Zhu, E. Chalmers, L. M. Chen, Y. Q. Wang, B. B. Xu, Y. Li and X. Q. Liu, *Small*, 2019, **15**, 1902440.
19 S. M. Burkinshaw and N. Kumar, *Dyes Pigm.*, 2009, **80**, 53–60.
20 J. L. Guo, Y. Ping, H. Ejima, K. Alt, M. Meissner, J. J. Richardson, Y. Yan, K. Peter, D. v. Elverfeldt, C. E. Hagemeyer and F. Caruso, *Angew. Chem., Int. Ed.*, 2014, **53**, 1–7.
21 R. Wang, X. X. Wang, Y. J. Zhan, Z. Xu, Z. Q. Xu, X. H. Feng, S. Li and H. Xu, *ACS Appl. Mater. Interfaces*, 2019, **11**, 37502–37512.
22 X. C. Du, L. Wu, H. Y. Yan, L. J. Qu, L. N. Wang, X. Wang, S. Ren, D. L. Kong and L. Y. Wang, *ACS Biomater. Sci. Eng.*, 2019, **5**, 2610–2620.
23 D. Yang, Y. F. Nia, X. X. Kong, D. H. Gao, Y. Wang, T. T. Hu and L. Q. Zhang, *Compos. Sci. Technol.*, 2019, **177**, 18–25.
24 S. Zhao, S. C. Xie, X. L. Liu, X. M. Shao, Z. Zhao, Z. X. Xin and L. Li, *J. Polym. Res.*, 2018, **25**, 225.
25 Y. He, C. L. Chen, G. Q. Xiao, F. Zhong, Y. Q. Wu and Z. He, *React. Funct. Polym.*, 2019, **137**, 104–115.

26 K. H. Hong, *Polym. Bull.*, 2017, **74**, 2861–2872.
27 W. L. Shang, Y. F. Rao, Y. Zheng, Y. Yang, Q. W. Hu, Z. Hu, J. Z. Yuan, H. G. Peng, K. Xiong, L. Tan, S. Li, J. M. Zhu, M. Li, X. M. Hu, X. H. Mao and X. C. Rao, *mBio*, 2019, **10**, e00880.
28 Z. Franks, R. A. Campbell, A. V. de Abreu, J. T. Holloway, J. E. Marvin, B. F. Kraemer, G. A. Zimmerman, A. S. Weyrich and M. T. Rondina, *Thromb. Haemostasis*, 2013, **109**, 684–695.
29 H. C. Chang, Y. T. Huang, C. S. Chen, Y. W. Chen, Y. T. Huang, J. C. Su, L. J. Teng, C. W. Shiau and H. C. Chiu, *J. Antimicrob. Chemother.*, 2016, **71**, 449–459.
30 U. T. Khatoon, G. N. Rao and M. K. Mohan, *J. Environ. Chem. Eng.*, 2018, **6**, 5837–5844.
31 R. Liu, H. W. Ge, X. Wang, J. Luo, Z. Q. Li and X. Y. Liu, *New J. Chem.*, 2016, **40**, 6332–6339.
32 J. Penders, M. Stolzoff, D. J. Hickey, M. Andersson and T. J. Webster, *Int. J. Nanomed.*, 2017, **12**, 2457–2468.
33 S. J. Ge, N. Ji, S. N. Cui, W. Xie, M. Li, Y. Li, L. Xiong and Q. J. Sun, *J. Agric. Food Chem.*, 2019, **67**, 11489–11497.
34 M. Szymanska-Chargot, A. Gruszecka, A. Smolira, K. Bederski, K. Głuch, J. Cytawa and L. Michalak, *J. Alloys Compd.*, 2009, **486**, 66–69.
35 Y. X. Gao, J. Hao, Q. Yan, F. P. Du, Y. Ju and J. Hu, *ACS Appl. Mater. Interfaces*, 2018, **10**, 17352.
36 M. Barthelemy, B. E. F. Gourbal, C. Gabrion and G. Petit, *Naturwissenschaften*, 2004, **91**, 135–138.
37 H. Meziane, A. M. Ouagazzal, L. Aubert, M. Wietrzych and W. Krezel, *Genes, Brain Behav.*, 2007, **6**, 192–200.
38 M. Korey, G. P. Mendis, J. P. Youngblood and J. A. Howarter, *J. Polym. Sci., Part A: Polym. Chem.*, 2018, **56**, 1468–1480.
39 Y. T. Xu, L. Li, X. X. Yu, Z. P. Gu and X. Zhang, *Carbohydr. Polym.*, 2012, **87**, 1589–1595.